EFFECT OF Fe DOPING VARIATION ON SIZE AND STRUCTURE IN COMPOSITE ZnS/CdS QUANTUM DOT TOWARDS EFFICIENCY IN ANTIMICROBIAL ACTIVITY

J. BARMAN[*], *B. BANIK*[**], *FARHANA SULTANA*[***]

[*]Department of Physics, ADP College, Nagaon, 782002, India, e-mail: jayantabarman2006@gmail.com
[**]Department of Herbal Science and Technology, ADP College, Nagaon, 782002, India
[***]Biotech Hub, ADP College, Nagaon, Assam, India

Abstract. Semiconductor material to biological system has a significant advance in recent research. The composite ZnS/CdS material with Fe doping has been grown by chemical route and there structural and composition has been analyzed by X-ray diffraction (XRD) and transmission electron microscopy (TEM). The surface was analyzed by scanning electron microscopy **(**SEM) and atomic force microscopy (AFM) method. The engineered band gap was calculated by absorption spectroscopy and found that absorption was blue-shifted. Photoluminescence analysis shows that luminescence of Fe^{2+} ions affected by the host crystal and symmetry leads to the emission color from green to orange/red. The band gap of the composite material depends on various parameter like doping concentration and composite material. From the established model the particles size was estimated and size becomes comparable with TEM and XRD. XRD patterns refined by the Rietveld method shows that the composite is hexagonal wurtzite structure. The structural analysis showed that doping concentration changes the size and transition level and create better efficiency in antimicrobial activity. The antibacterial observation showed that the 2.0 wt% Fe-doped with composite 2:3 ratio exhibited maximum antibacterial effect.

Key words: Composite, antimicrobial, XRD.

INTRODUCTION

The composite semiconducting and magnetic material has lost of importance due to their large application in optoelectronic and biological process. Composite material has unique relevance to biomedical applications due to their ultra-small size with cell (5–50 μm), viruses (10–500 nm), proteins (10–50 nm) and gene (10–100 nm) [7, 15, 27]. Semiconductor and magnetic biomaterials have different challenges for application in biological point of view. The surface to volume ratio of the nanostructured exhibit potent antibacterial properties due to physical, chemical and biological properties that develop with tuneable size effects [2, 5, 8,

Received: May 2021;
in final form July 2021.

ROMANIAN J. BIOPHYS., Vol. 31, No. 4, P. 165–175, BUCHAREST, 2021

11]. Among the various compound semiconductor, zinc sulphide and cadmium sulphide nanoparticles have been found to be very effective antibacterial activity. Studies have shown that metal oxide nanoparticles such as ZnS and CdS NPs, have selective toxicity to bacteria and exhibit minimum effect on human cells [21, 24]. ZnS, being a wide band gap (3.37 eV) and CdS (2.42 eV) wurtzite-phase semiconductor, which has attracted a considerable scientific attention, due to its importance of suitable band gap and applications in the fields of opto-electronics properties [28]. The trap states inside the band gap were analyzed to recognize the sub-bandgap energy levels [9]. The defect level plays an important role in various properties like luminescence and chemical activity with fast photo absorption, transportation, and collection [23].

Photoluminescent properties of blue emission band centered at 418 nm in composite material is due to the host related defect states like Zn vacancies [26]. The suppressed green emission due to the incorporation of Fe^{2+} ions which is effective in antimicrobial activity.

In developing countries, the bacterial contamination of drinking water becomes a major issue. The removal or inactivation of pathogenic microorganisms is important in water treatment. Application in semiconductor nanoparticles is the promising area for removal of microorganism due to the high chemical affinity with photocatalytic activity [12]. Lots of research is under process for purification of drinking water.

MATERIALS AND METHODS

The composite semiconductor biomaterials have different challenges than material used for other application. *In vivo* applications required strict biocompatibility. *In vitro* applications have less strict, but techniques involving living cell must consider the effect the material on the sample under the study.

CHEMICAL PROCESS FOR COMPOSITE MATERIAL WITH DOPPING

Un-doped and Fe-doped of composite ZnS/CdS nanoparticles with 0.5, 1.0, 1.5, and 2.0 wt% of Fe were synthesized by chemical method using ZnS, NaOH, $CdCl_2$ and Na_2S. All the materials used were of analytic grade obtained from Merck, India, and used without further purification. The constituent in the desired proportions were dissolved in deionized water and stirred for 12 hours to obtain a clear transparent solution. It was then poured into a silica crucible, and then placed in a domestic microwave-oven and exposed to the microwave energy. The obtained samples were thoroughly washed with alcohol for several times to remove the ions possibly remaining in the final products and then dried in a hot air oven at 70 °C for 2 hours. After preparation solution was caste in glass substrate and kept 24 hours for adhesion.

TEST AND PROCESS FOR ANTIBACTERIAL ACTIVITY

E. coli (MTCC 739), *Klebsiella pneumonia* (MTCC 432), *Pseudomonas aeruginosa* (MTCC-424) were used for antibacterial activity. The bacterial cultures were maintained on nutrient agar slants and kept at –4 °C.

1 mg of composite sample was weighed to prepare a solution of 1 mg/mL concentration. Antibacterial activity is performed in both doped and undoped composite. The pathogenic samples were cut in 8 mm diameter and added in composite material for inhibitory controls of gram-negative and gram-positive bacteria. All arrangement is performed at 37 °C for 24 h. After incubation period diameters were measured with high resolution travelling microscope. The data are analyzed using Origin graphic software.

RESULTS

XRD BY RIETVELD REFINEMENT TECHNIQUE

Fe doped ZnS/CdS nanoparticles was prepared in powered form and analyzed by X'Pert Pro X-ray diffractometer operated at a voltage of 40 kV and a current of 30 mA with Cu Kα radiation. The diffraction peaks are obtained at 2θ = 28.73 °, 31.38 °, 37.22 °, 47.56 °, 57.59 °, 63.79 °, 67.43 °, 68.95 °, 70.08 °, 72.67 °, and 77.05 °. The corresponding planes are (100), (002), (101), (102), (110), (103), (200), (112), (201), (004), (202) respectively. The diffraction peaks are indexed with the hexagonal wurtzite type structure (phase Zincite, syn). The sharp and intense peaks indicate the high crystallinity of the sample. It shows the that Fe^{2+} ions were systematically substituted into Zn^{2+} ions sites within the ZnS and CdS crystal lattice without changing the parent structure of composite which is in good agreement with the one reported earlier [17]. When samples were doped with Fe the peaks are broaden and shifted to higher diffraction angle indicates that particle size becomes smaller. The average crystallite size was estimated using Debyee Scherrer equation [4]. The average crystallite size of Fe doped ZnS/CdS NPs was found to be in the range of 5–8 nm. Refinement plots of Fe-doped ZnS/CdS nanoparticles are shown in Fig. 1. Refinement is based on the factor $S = Rwp/Re$, where, S indicates crystalline size, R is Rietveld factor, Rwp and Re are R weighted and R-expected patterns, respectively. The increasing of lattice parameters clearly indicates that Fe^{2+} ions are substituting Zn^{2+} ions on the ZnS and Cd^{2+} in CdS matrix [16].

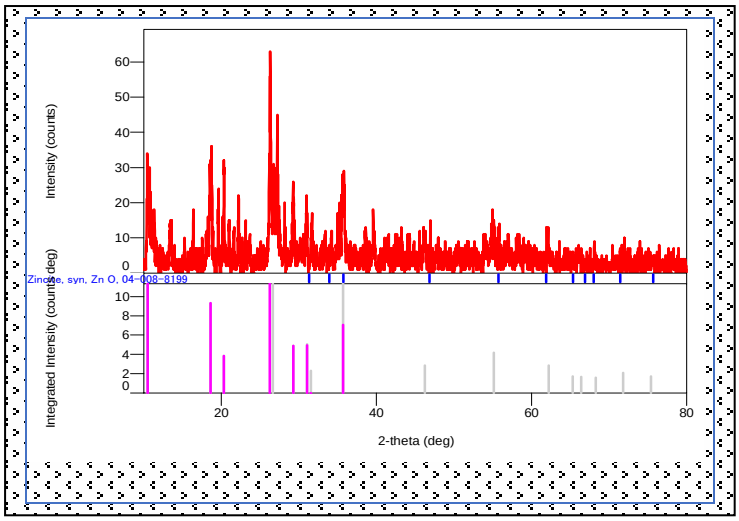

Fig. 1. XRD rietveld refinement spectrum of Fe doped ZnS/CdS.

Table 1

Fe doped ZnS/CdS angular correction

A (Å)	B (Å)	C (Å)	Alpha (deg)	Beta (deg)	Gamma (deg)
3.268(6)	3.268(6)	5.260(11)	90.000000	90.000000	120.000000

Table 2

Fe doped ZnS/CdS structure parameters

Rwp (%)	*Rp* (%)	*Re* (%)	*S* (%)	Chi^2	Maximum shift/e.s.d.
64.5600	55.4100	44.3200	1.3732	2.2643	0.0830

The *RR* analysis gives the information about the variation of lattice parameters a and c, as a function of dopant concentration. In Table 2, *Rp* represents the refinement fitting profile. The calculated lattice parameters are shown in Table 1 and structural parameter are shown in Table 2.

TEM RESULT ANALYSIS

The size of the particle was confirmed by HRTEM with direct image technique (Model-JEM-100 CX II, Jeol). Fig. 2 shows the different condition of the Fe doped ZnS/CdS nanocomposite. It is clear that size of the particles is uniform and uniformly distributed doped ZnS/CdS nanostructure showed that the sample

had an average diameter 30 nm. From lots of observations, it is found that size of the particle depends on doping concentration and decreases when doping concentration increases which is a good agreement with optical effective mass approximation model.

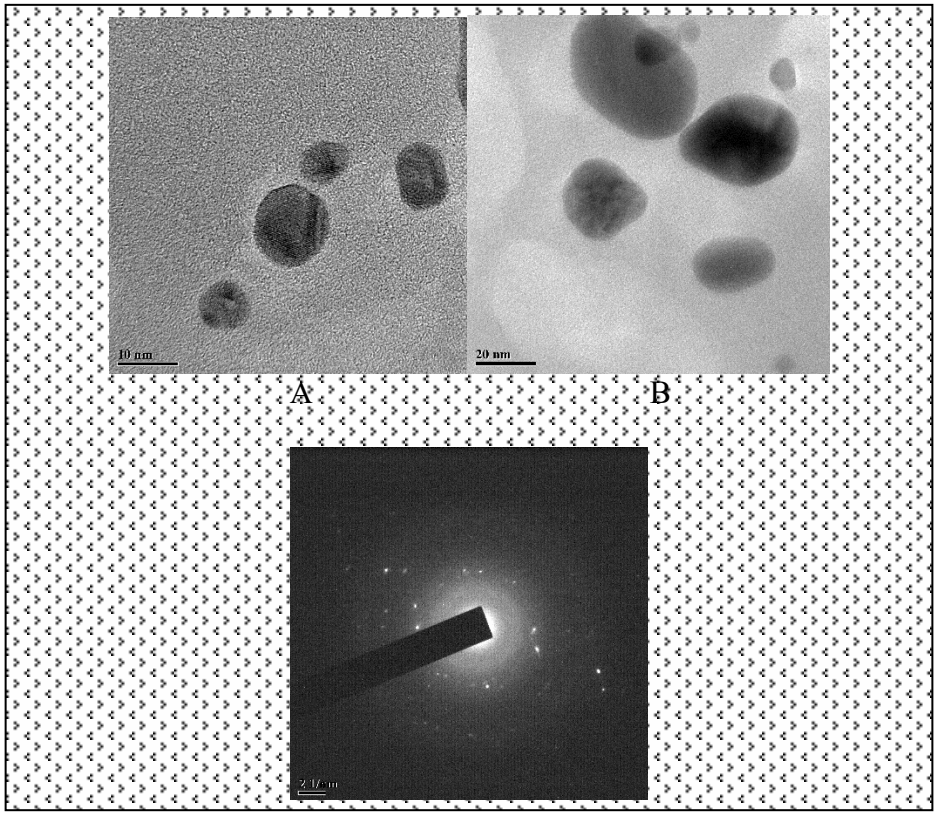

Fig. 2. TEM micrograph of ZnS/CdS nanoparticle (A) without doping, (B) after Fe doping, and (C) SAED pattern of the one-dimensional Fe dopped ZnS/CdS.

SEM AND AFM RESULT ANALYSIS

Fig. 3(A) shows surface topography of ZnS/CdS composite and Fig. 3(B) 2.0 wt% Fe-doped ZnS/CdS nanoparticles size ranging from 37 to 42 nm.

It is observed that hexagonal grains are uniformly distributed at the surface. A slight decrease of the grain size is observed when doping concentration increases and the surface roughness remains same. From the SEM the particles are seen to be almost symmetrical. It is observed that when the sample is kept for long time exposer of electron beam agglomeration takes place and as a result size and shape of the sample changes.

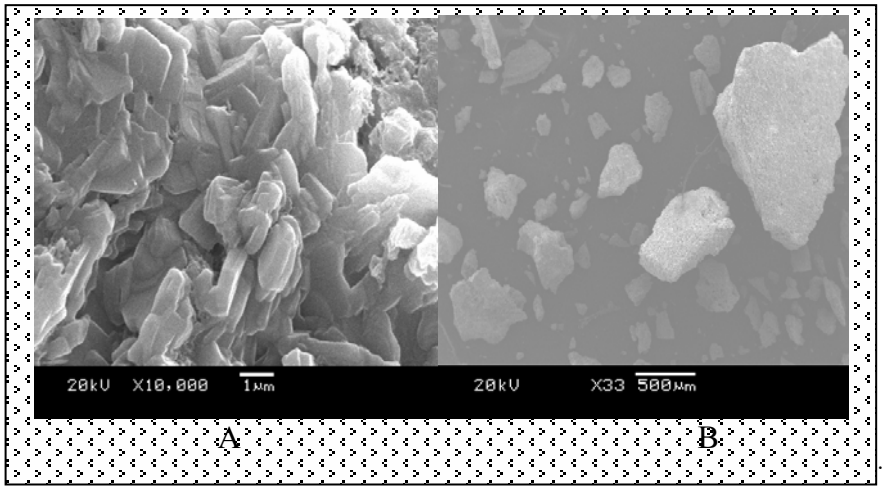

Fig. 3. SEM image of ZnS/CdS nanoparticle (A) without doping (B) 2.0 wt% Fe-doped ZnS/CdS.

Fig. 4 shows the AFM 2.0 wt% Fe-doped ZnS/CdS nanoparticles. The AFM measurements are performed in contact mode in air by using a molecular imaging microscope (model PICO Scan 2500). The cantilever force constant 0.21 N/m was used and shows the 2D AFM image of composite nanoparticles of area 3000 nm × 3000 nm. The surface appears nearly smooth as observed by AFM.

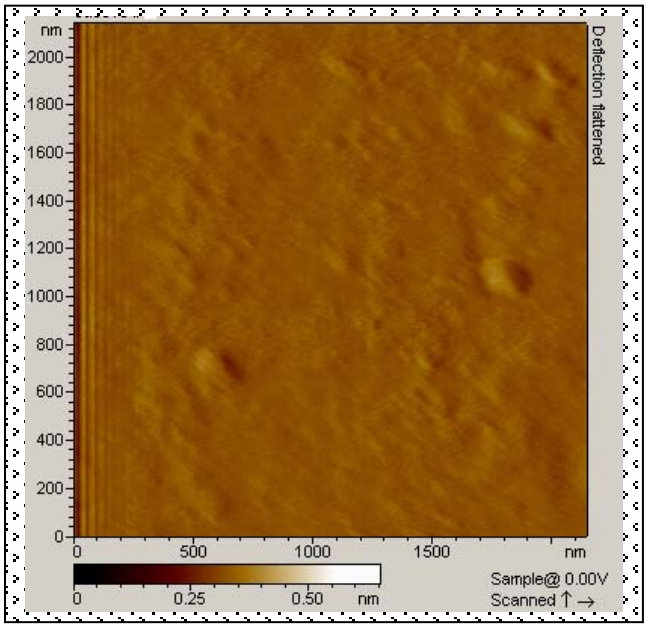

Fig. 4. 2D AFM image at 2.0 wt% Fe-doped ZnS/CdS nanoparticles.

PHOTOLUMINESCENCE STUDIES

Fig. 5 shows the room temperature PL spectrum of Fe^{2+} doped ZnS/CdS nanocomposite and the excitation wavelength of 325 nm. Luminescence of Fe^{2+} ions affected by the mother crystal structure and emission color becomes green to orange/red.

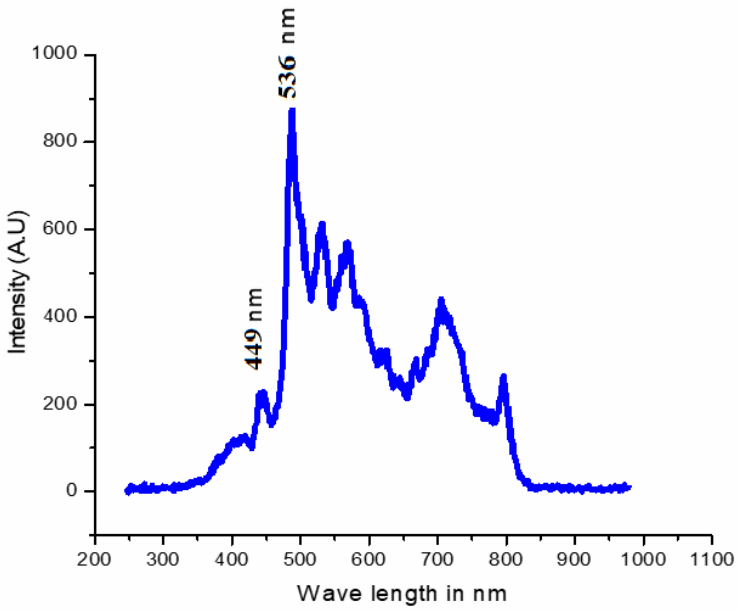

Fig. 5. Photoluminescence image Fe-doped ZnS/CdS nanoparticles.

PL spectrum exhibits five characteristic and reveal the presence of two main peaks region is at 449 nm and visible region at 536 nm. Emission in 449 nm is due to the exciton recombination. The blue emission is due to the doping and trapping within the crystal. The Cd and Zn vacancy creates green emission [1, 6, 14, 18, 22].

UV ANALYSIS

UV-Vis spectrum was recorded in the range 300 to 800 nm; it is shown in Fig. 6.

In the composite material CdS and ZnS has direct band gap 3.7 eV and 4.0 eV. In the Fig. 6, A is undoped condition and B and C is the doping condition at concentration level 2 % and 3 %, respectively. It is found that at higher doping level ban gap increases and as result particle size decreases.

The stability of synthesized particles is recorded at intervals of 1, 15 and 30 days after storage at ambient temperature. There was no obvious change in peak position for two weeks.

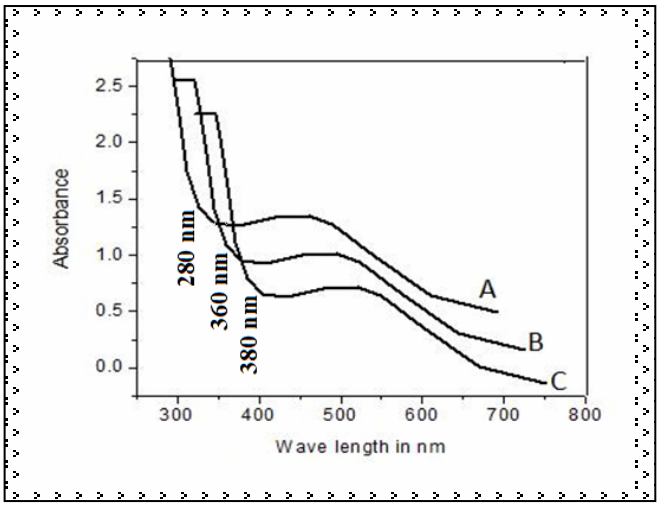

Fig. 6. UV-Vis absorption spectrum of Fe doped ZnS/CdS nanoparticle.

To calculate the possible transition, $(\alpha h\upsilon)^2$ *versus* $h\upsilon$ were plotted (Fig. 7) and corresponding band gaps were obtained by extrapolating the straight-line portion of the curves to $(\alpha h\upsilon)^2 = 0$. Using the established optical model size of the particle determined which is a good agreement with HRTEM.

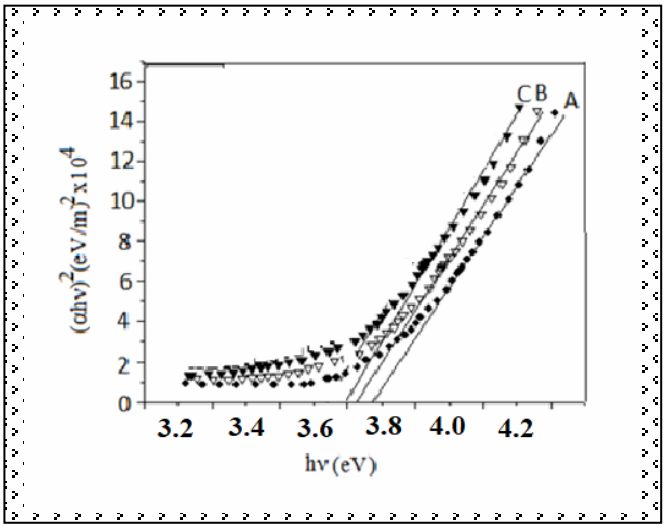

Fig. 7. Band gap of different composite ratio of ZnO/CdS with Fe doping.

$$E_{gn} = [\, E^2_{gb} + 2\hbar^2 E_{gb}(\pi/R)^2 / m^*]^{1/2} \quad (1)$$

where m^* is the average effective mass of the composite, E_{gb} is the bulk band gap of both ZnS and CdS and E_{gn} is the calculated band gap energy [3, 10, 13, 19, 20, 25]. The average particle size was found in the range 4–9 nm. Table 3 shows the amount of band gap energy and blue shift energy with concentration.

Table 3

Optimum composition ratio of Fe doped ZnS/CdS

Sample no.	**Doping concentration**	**Band gap energy (eV)**	**Blue shift energy (eV)**
(a)	undoped	3.8	0.12
(b)	2 wt%	3.97	0.29
(c)	3 wt%	4.02	0.34

ANTIMICROBIAL ACTIVITY

Antibacterial activity of composite material with doped and undoped are carried out with three water borne pathogenic bacteria. Tetracycline of 1mg/mL concentration was used as a control antibacterial agent. Activity was determined on the basis of inhabitation area. Antimicrobial activity increases when particle size is decreases and doping concentration increases [20]. Table 4 shows the type of bacterial strain and zone of inhibition in nm along with dopped and undoped condition. Significant change was analyzed by one-way analysis of variance followed by Dunnett's multiple comparisons test using Graph Pad Instat Software; $^{**}P < 0.01$ compared to standard control.

Table 4

Antibacterial efficacy of ZnS/CdS nanoparticles and standard antibiotic against three bacterial strains. Values are plotted as the mean±SEM, $n = 5$, in each group

Types of bacterial strains	**Zone of inhibition (in mm)**						**Tetracyclin (1 g·mL^{-1})**
	Fe ZnS/CdS nanoparticles			**Undoped ZnS/CdS nanoparticles**			
	30 µL	70 µL	100 µL	30 µL	70 µL	100 µL	100 µL
E. coli	5.00±0.14	11.00±0.11	18.00±0.13	6.00±0.14	11.00±0.11	20.00±0.11	35.00±0.08
K. pneumonia	8.00±0.11	12.00±0.16	20.00±0.15	9.00±0.13	11.00±0.16	22.00±0.13	32.00±0.09
P. aeruginosa	2.00±0.15	9.00±0.14	17.00±0.11	4.00±0.15	9.00±0.15	17.00±0.11	31.00±0.09

CONCLUSIONS

Fe doped composite ZnS/CdS successfully synthesized by chemical method. The prepared sample is composed of two phases. Overlapping and void created in the crystal due to the ionic radii of Fe^{2+}, Zn^{2+} and Cd^{2+} mismatching and leads to very slight shift in the main characteristic peaks of XRD pattern. The optimum ratio of ZnS and CdS found to be 2:3 for better antimicrobial activity. Optical band gap was calculated for different doping concentration Fe and ZnS/CdS compositions ratio and band gap changes from 3.7 to 3.9 eV. This current study was aimed to analyze the vital application of ZnS/CdS-NPs as antimicrobial agent for water treatment and efficient antimicrobial effect was found when size of the particles becomes smaller and smaller. The zone inhabitation found optimum when doping concentration becomes 2 wt% in the ratio of composite 2:3.

Acknowledgements. The author would like to acknowledge ASTEC project and Star College Scheme Govt of India (DBT) for financial assistance. We would also like to acknowledge NEHU and NIT Nagaland, GU for providing us TEM, SEM and XRD facilities respectively.

REFERENCES

1. ANSARI, S.A., A. NISAR, B. FATMA, W. KHAN, A.H. NAQVI, Investigation on structural, optical and dielectric properties of Co doped ZnO nanoparticles synthesized by gel-combustion route, *Mater. Sci. Eng. B*, 2012, **177**, 428–435.
2. BRAYNER, R., R. FERRARI-ILIOU, N. BRIVOIS, S. DJEDIAT, M.F. BENEDETTI, F. FIEVET, Toxicological impact studies based on *Escherichia coli* bacteria in ultrafine ZnO nanoparticles colloidal medium, *Nano Lett.*, 2006, **6**, 866–870.
3. CAGLAR, Y., Sol-gel derived nanostructure undoped and cobalt doped ZnO: Structural, optical and electrical studies, *J. Alloy Compd.*, 2013, **560**, 181−188.
4. CHEN, Y., Q. TAO, W. FU, H. YANG, X. ZHOU, Y. ZHANG, S. SU, P. WANG, M. LI, Enhanced solar cell efficiency and stability using ZnS passivation layer for CdS quantum-dot sensitized actinomorphic hexagonal columnar ZnO, *Electrochim. Acta*, 2014, **118**, 176–181.
5. GENG, T., S. ZHANG, Y. CHEN, Study on the synthesis and photocatalysis of Ag_3PO_4 polyhedral microcrystals, *Bull. Mater. Sci.*, 2020, **43**, 223−230.
6. HSU, S.H., S.F. HUNG, S.H. CHIEN, CdS sensitized vertically aligned single crystal TiO_2 nanorods on transparent conducting glass with improved solar cell efficiency and stability using ZnS passivation layer, *J. Power Sources*, 2013, **233**, 236–243.
7. IRIMPAN, L., V.P.N. NAMPOORI, P. RADHAKRISHNAN, Spectral and nonlinear optical characteristics of nanocomposites of ZnO-CdS, *J. Appl. Phys.*, 2008, **103**, 094914.
8. JANA, T.K., A. PAL, K. CHATTERJEE, Self-assembled flower like CdS-ZnO nanocomposite and its photo catalytic activity, *J. Alloys Compd.*, 2014, **583**, 510–515.
9. KAJBAFVALA, A., H. GHORBANI, A. PARAVAR, J.P. SAMBERG, E. KAJBAFVALA, S.K. SADRNEZHAAD, Effect of morphology on photocatalytic performance of Zinc oxide nanostructures synthesized by rapid microwave irradiation methods, *Superlattices Microstruct.*, 2012, **52**, 512–522.
10. KHAN, I., S. KHAN, R. NONGJAI, H. AHMED, W. KHAN, Structural and optical properties of gel-combustion synthesized Zr doped ZnO nanoparticles, *Opt. Mater*, 2013, **35**(6), 1189−1193.

11. LIU, J., K. ZHU, B. SHENG, Z. LI, G. TAI, J. QIU, J. WANG, J. CHEN, Y. YOU, Q. GU, P. LIU, Low-temperature solid-state synthesis and optical properties of ZnO/CdS nanocomposites, *J. Alloys Compd.*, 2015, **618**, 67–72.
12. LUO, L.J., W. TAO, X.Y. HU, T. XIAO, B.J. HENG, W. HUANG, H. WANG, H.W. HAN, Q.K. JIANG, J.B. WANG, Y.W. TANG, Mesoporous F-doped ZnO prism array with significantly enhanced photovoltaic performance for dye-sensitized solar cells, *J. Power Sources*, 2011, **196**, 10518–10525.
13. MISRA, M., P. KAPUR, C. GHANSHYAM, M.L. SINGLA, ZnO@ CdS core–shell thin film: fabrication and enhancement of exciton life time by CdS nanoparticle, *J. Mater. Sci. Mater. Electron.*, 2013, **24**, 3800–3804.
14. MOHAPATRA, J., D.K. MISRA, D. MISRA, A. PERUMAL, V.R.R. MEDICHERLA, D.M. PHASE, S.K. SINGH, Room temperature ferromagnetism in Co doped ZnO within an optimal doping level of 5 %, *Mater. Res. Bull.*, 2012, **47**, 1417–1422.
15. NAYAK, J., S.N. SAHU, J. KASUYA, S. NOZAKI, CdS-ZnO composite nanorods: Synthesis, characterization and application for photocatalytic degradation of 3,4-dihydroxy benzoic acid, *Appl. Surf. Sci*, 2008, **254**, 7215–7218.
16. PARK, Y.C., E.H. KONG, Y.J. CHANG, B.G. KUM, H.M. JANG, Tertiary hierarchically structured TiO_2 for CdS quantum-dot-sensitized solar cells, *Electrochim. Acta*, 2011, **56**, 7371–7376.
17. PAWAR, B.N., G. CAI, D. HAMA, R.S. MANE, T. GANESH, A. GHULE, R. SHARMA, K.D. JADHAVA, S.H. HAN, Preparation of transparent and conducting boron doped ZnO electrode for its application in dye sensitized solar cells, *Sol. Energy Mater. Sol. Cells*, 2009, **93**, 524–527.
18. PEREZ, C., M. PAUL, P. BAZERAUE, Antibiotic assay by agar well diffusion method, *Acta Biol. Med. Exp.*, 1990, **15**, 113–115.
19. RAO, G.T., B. BABU, R.J. STELLA, V.P. MANJARI, C.V. REDDY, S. JAESOOL, R.V.S.S.N. RAVIKUMAR, Synthesis and characterization of VO_2^+doped ZnO-CdS composite nanopowder, *J. Mol. Struct.*, 2015, **1081**, 254–259.
20. REDDY, A.J., M.K. KOKILA, H. NAGABHUSHANA, J.L. RAO, B.M. NAGABHUSHANA, C. SHIV-AKUMARA, R.P.S. CHAKRADHAR, EPR and photoluminescence studies of ZnO:Mn nanophosphors prepared by solution combustion route, *Spectrochim. Acta A*, 2011, **79**, 476–480.
21. REDDY, K.M., K. FERIS, J. BELL, D.G. WINGETT, C. HANLEY, A. PUNNOOSE, Selective toxicity of zinc oxide nanoparticles to prokaryotic and eukaryotic systems, *Appl. Phys. Let.*, 2007, **90**, 2139021–2139023.
22. SATO, K., K. KATAYAMA, H. YOSHIDA, Zener model description of ferromagnetism in zinc-blende magnetic semiconductors, *Jpn. J. Appl. Phys.*, 2000, **39**, 555–558.
23. TARWAL, N.L., R.S. DEVAN, Y.R. MA, R.S. PATIL, M.M. KARANJKAR, P.S. PATIL, Spray deposited localized surface plasmonic Au-ZnO nanocomposites for solar cell application, *Electrochim. Acta,* 2012, **72**, 32–39.
24. THILL, A., O. ZEYONS, O. SPALLA, F. CHAUVAT, J. ROSE, M. AUFFAN, A.M. FLANK, Cytotoxicity of CeO_2 nanoparticles for *Escherichia coli* physico-chemical insight of the cytotoxicity mechanism, *Environ. Sci. Technol.*, 2006, **40**, 6151–6156.
25. WU, D., Z. HUANG, G. YIN, Y. YAO, X. LIAO, D. HAN, X. HUANG, J. GU, Preparation structure and properties of Mn-doped ZnO rod arrays, *Cryst. Eng. Comm.*, 2010, **12**, 192–198.
26. YANG, W.F., Z.Y. WU, Z.G. LIU, L.M. KONG, Deposition of Ni, Ag, and Pt-based Al-doped ZnO double films for the transparent conductive electrodes by RF magnetron sputtering, *Appl. Surf. Sci.*, 2010, **256**, 7591–7595.
27. YUAN, K., L. CHEN, F. LI, Y. CHEN, Nanostructured hybrid ZnO@CdS nanowalls grown *in situ* for inverted polymer solar cells, *J. Mater. Chem. C,* 2, 2014, **6**, 1018–1027.
28. ZHANG, L.L., Y.H. JIANG, Y.L. DING, M. POVEY, D. YORK, Investigation into the antibacterial behavior of suspensions of ZnO nanoparticles (ZnO nanofluids), *J. Nanopart. Res.*, 2007, **9**, 479–489.